Two-photon excitation of the lowest $4f \rightarrow 5d$ near-ultraviolet transition in Ce^{3+}:CaF_2

S. K. Gayen and D. S. Hamilton
Department of Physics and Institute of Materials Science, University of Connecticut, Storrs, Connecticut 06268
(Received 8 June 1983)

The two-photon transition from the $4f$ ground state to the lowest Ce^{3+} $5d$ state in Ce^{3+}:CaF_2 has been studied with a tunable dye laser as a function of laser wavelength, intensity, polarization, and focusing geometry. At liquid-helium temperatures, a no-phonon resonance line is observed and is accompanied by its vibrational sideband. The peak cross section for the two-photon absorption is of order 5×10^{-54} cm^4 sec, indicating significant crystal-field parity mixing for the $5d$ levels. The no-phonon line shows a polarization anisotropy consistent with a Ce^{3+} site of C_{4v} symmetry. The phonon sideband has a frequency-dependent polarization anisotropy.

I. INTRODUCTION

The advent of laser sources for use in solid-state spectroscopy has made possible the observation of multiphoton-absorption processes in impurity-ion–doped insulators.[1–11] For the most part, the investigations reported to date have studied sharp parity-allowed resonance transitions in these materials. In this paper we report on a first-order parity-forbidden two-photon transition in Ce^{3+}:CaF_2 for which a sharp no-phonon resonance and its broad phonon sideband are observed simultaneously with comparable strength.

The Ce^{3+}:CaF_2 system has a number of characteristics which prove advantageous for this investigation. The Ce^{3+} ion has a single optically active electron so that its energy-level diagram is relatively simple and the number of states participating in a second-order optical process is small. A wide variety of background information on the Ce^{3+}:CaF_2 crystal is available including one-photon absorption and fluorescence spectra,[12–15] electron-nuclear double resonance (ENDOR),[16] EPR,[17] and Zeeman[18] and Stark[19] measurements. In low-concentration and oxygen-free samples, the dominant site symmetry of the Ce^{3+} ion is C_{4v}. Here the Ce^{3+} ion substitutes for a Ca^{2+} ion with an interstitial F^- charge compensator in the adjacent cell, inducing the tetragonal distortion. The C_{4v} crystal-field and spin-orbit coupling splits the $5d$ free-ion orbital into five widely spaced nondegenerate levels lying in the near-ultraviolet region. The $4f$ level splits into the $^2F_{5/2}$ and $^2F_{7/2}$ manifolds separated by about 2000 cm^{-1}. The transition studied here is from the lowest Stark component of the $^2F_{5/2}$ manifold to the lowest state of the $5d$ configuration.

We have observed a purely electronic two-photon absorptive transition by the Ce^{3+} ions along with its phonon sideband. Since the $4f$ and $5d$ states have opposite parity, a two-photon transition between them is electric dipole forbidden. However, at the noncentrosymmetric C_{4v} site of the Ce^{3+} ion, the odd crystal-field component lifts the parity selection rule for the no-phonon transition. To observe the two-photon transitions, we have chosen to detect the fluorescence emission of the excited Ce^{3+} ions rather than to monitor the intensity change of a transmitted probe beam. Since the energy gap between the $5d$ and the $4f$ states is some 30 000 cm^{-1}, the quantum efficiency of fluorescence is high. In addition, the emission is over a limited wavelength interval far from the excitation wavelength. These facts serve to optimize our sensitivity for observing weak two-photon transitions in low Ce^{3+}-concentration samples.

II. EXPERIMENTAL APPARATUS

The experimental arrangement for two-photon excitation spectroscopy is shown in Fig. 1. The two-photon transitions were measured by monitoring the broadband [(310–355-nm)] Ce^{3+} fluorescence following excitation by a 5-nsec pulse from a tunable dye laser pumped by a Nd:YAG (yttrium aluminum garnet) laser (Quanta-Ray DCR-1). The dye laser uses a dual-prism beam expander and a 600-line/mm blazed grating in Littrow to produce 0.1-cm^{-1} bandwidth pulses with a 99% polarization ratio. A 50-cm-focal-length spherical aberration and coma-corrected doublet focused the dye-laser beam into the sample.

The Ce^{3+}:CaF_2 samples used in the experiment were obtained from Optovac Inc. and were grown by a slow anneal Bridgman-Stockbarger method. The crystals were in the form of cylinders 4 mm long and 10 mm in diameter with the [100], [110], or [111] axis of the cubic CaF_2 parallel to the cylinder axis. These samples were then x-ray oriented by Laue backreflection. The [100]-axis crystal was cut and polished along planes orthogonal to the

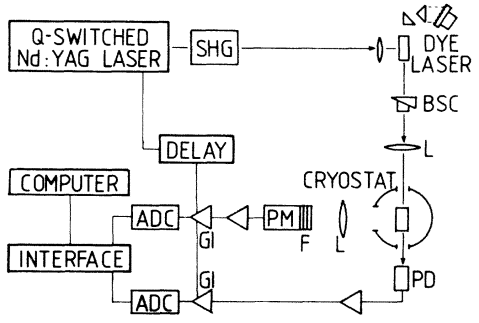

FIG. 1. Schematic representation of the experimental setup for two-photon excitation spectroscopy.

 ©1983 The American Physical Society

[100] axis and the [001] axis, the [110] crystal along planes orthogonal to the [110] and [1$\bar{1}$0] axes, and the [111] crystal along planes orthogonal to the [111] and [1$\bar{1}$0] axes. The samples were mounted on a cold finger in the tail section of a continuous liquid-helium flow cryostat. The alignment of the sample axes with respect to the horizontal laser beam and a vertical reference direction was accurate to ± 2 degrees. A Babinet-Soleil compensator was adjusted to a half-wave retardation and was used to control the angle between the linearly polarized laser field and the CaF_2 axes.

The fluorescence was collected at right angles to the laser beam by a 5-cm-diam. fused quartz lens located 10 cm from the sample and passed through three Schott UG5 filters. Each filter has a transmission coefficient of 0.8 over most of the Ce^{3+} fluorescence band and 10^{-5} at the dye-laser wavelengths. The fluorescence was detected by a blue-enhanced EMI 9781-B photomultiplier tube. An HP-5082-4203 photodiode, calibrated against a Laser Precision model 7000 Joulemeter, monitored the changes in the dye-laser pulse energy. Since the absorptive loss of the the laser beam through the sample is negligible, the photodiode can be located after the sample. Both the photodiode and photomultiplier current outputs were integrated by collecting capacitors which, in parallel with a resistor, provide a voltage output with a 50-μsec decay time. These signals were sensed by identical gated integrators (Evans 4130) whose outputs were digitized by 12 bit analog to digital converters and accumulated by an Apple II minicomputer. Two Canberra 2055 delay modules were used to synchronize the laser and gated integrator timing.

Three different dyes (DCM, Rhodamine 101, and Kiton Red) were used to provide overlapping spectra between 615 and 590 nm. Because of the variations in the dye-laser pulse energy, the fluorescence signal was normalized by the square of the dye-laser reference voltage for each laser shot. The random fluctuations in the temporal profile of the pulsed dye laser necessitated computer averaging of the normalized signal over 50 laser shots at each wavelength to achieve an adequate signal-to-noise ratio. By recording the data in this way we found that our results were very reproducible in the overlapping wavelength regions of different dyes and that no scale parameters were needed to produce the composite two-photon excitation spectra. The minicomputer was also interfaced to control the dye-laser wavelength through a stepping motor connected to the grating drive mechanism. Hard copy output of the spectra was obtained from a computer-controlled plotter or printer and was saved on magnetic tape.

We have complemented the two-photon excitation spectra with the one-photon excitation spectra. For these measurements the laser system was replaced by a Xe lamp and a $\frac{1}{4}$-m Jarrel-Ash monochromator. The exciting light was amplitude modulated by a 440-Hz chopper wheel and a PAR model 121 lock-in amplifier detected the output of the photomultiplier. An additional filter (Schott WG-335) was used to ensure that none of the exciting light reached the photomultiplier. The minicomputer was used to step the monochromator to new wavelengths and to read the voltage output of the lock-in amplifier.

III. EXPERIMENTAL RESULTS

A. One- and two-photon excitation spectra

The one-photon excitation spectrum taken at a 6-K sample temperature is shown in Fig. 2. The sharp resonance at 313.2 nm is a no-phonon transition and it is accompanied by its phonon sideband extending beyond 290.0 nm. The very close similarity between this excitation spectrum and published absorption spectra[13–15] indicates that the quantum efficiency of fluorescence is independent of the number and frequency of the participating phonons. Hence the two-photon excitation spectrum is also expected to be identical to a two-photon absorption spectrum over the same band.

The two-photon excitation spectrum is shown in Fig. 3. At liquid-helium temperature, a sharp peak [0.64 cm^{-1} full width at half maximum (FWHM)] is observed when the dye laser is tuned through 626.4 nm. Since the one-photon excitation and absorption spectra show a sharp no-phonon line at 313.2 nm, we conclude that a two-photon absorption process causing a purely electronic transition from the $4f$ ground state to the lowest $5d$ state of the Ce^{3+} ions is responsible for the 626.4-nm peak. The decay time of the fluorescence for both the one- and two-photon pumping is about 25 nsec as expected for the $5d \rightarrow 4f$ radiative relaxation of the excited Ce^{3+} ions. As the dye laser is tuned to shorter wavelengths, a broad but structured band is seen to accompany the sharp 626.4-nm no-phonon line. We interpret this feature as the phonon sideband of this $4f \rightarrow 5d$ two-photon transition. A comparison of the one- and two-photon excitation spectra shows significant correlation in the structure of the two sidebands.

To verify the two-photon nature of the absorption, we have monitored the fluorescence strength as a function of the dye-laser power. By using a series of calibrated neutral density filters in the dye-laser beam, we have avoided the systematic errors associated with controlling the dye-laser power by varying the YAG laser lamp energy. The results displayed in Fig. 4 show a quadratic dependence as expected for a two-photon absorption.

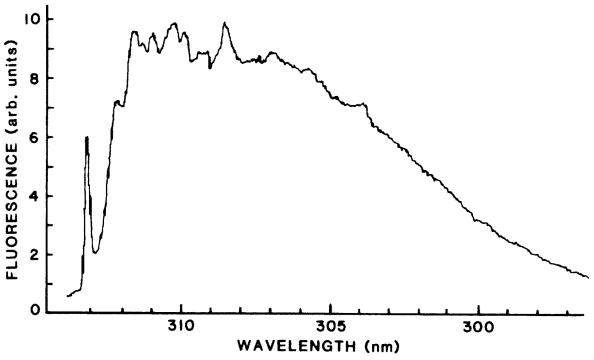

FIG. 2. One-photon excitation spectrum of 0.003% Ce^{3+}:CaF_2 at 6 K. The resolution of the monochromator was 0.2 nm.

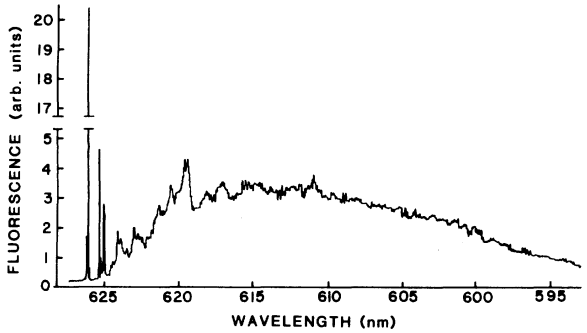

FIG. 3. Composite two-photon excitation spectrum of 0.003% Ce^{3+}:CaF_2 at 6 K. The fluorescence intensity has been point by point normalized to the square of the dye-laser power. The dye-laser beam is along the [100] axis and is linearly polarized along the [010] direction. The sharp lines just to the right of the dominant no-phonon line are presumably due to Ce^{3+} ions at slightly perturbed lattice sites.

B. Absolute cross-section measurement

For a laser photon flux F in photons/cm^2 sec, the transition rate per ion for a two-photon absorption is

$$W=\sigma F^2 , \tag{1}$$

where σ is the two-photon cross section in cm^4 sec. If ρ is the Ce^{3+} density (ions/cm^3) then the number of ions excited per laser pulse of length T is

$$N=T\rho\sigma\int_0^R\int_{-L/2}^{L/2}F^2(r,z)2\pi r\,dr\,dz , \tag{2}$$

where the integral is over the sample of length L and radius R. Although the dye-laser beam is multimode, a spatial scan of a narrow slit or pinhole across the beam shows that the flux distribution can be approximated by a Gaussian

$$F(r,z)=\frac{2P}{\pi w^2}\exp\left[-\frac{2r^2}{w^2}\right] . \tag{3}$$

The power is P in photons/sec and w is the z-dependent beam radius. We also find that the focusing characteristics of the beam are well approximated by

$$w^2(z)=w_0^2\left[1+\left[\frac{z-z_0}{b/2}\right]^2\right] , \tag{4}$$

where the minimum beam radius w_0 is at $z=z_0$ and the confocal parameter is $b=2\pi w_0^2/\lambda$. With the use of these descriptions for $F(r,z)$ and $w(z)$, the integral in Eq. (2) becomes[20]

$$N=\frac{T\rho\sigma P^2}{\lambda}\left[\tan^{-1}\left[\frac{L-2z_0}{b}\right]+\tan^{-1}\left[\frac{L+2z_0}{b}\right]\right] . \tag{5}$$

The dependence of N on z_0 can be used as a simple way of determining an effective minimum waist w_0. With the use of the geometry of Fig. 5, z_0 can be related to the lens to minimum-waist distance d_2 and the lens to sample separation x. In far field of the dye laser the value of d_2 is nearly independent of d_1 and we can vary z_0 by moving the lens instead of the sample.[21] In Fig. 6, the results of measuring the Ce^{3+} fluorescence signal as a function of z_0 are shown with a fit to the bracketed term in Eq. (5) for $b=2.1$ cm ($w_0=45$ μm). This effective waist parameter agrees well with a 50-μm value estimated from scanning a 10-μm slit across the focal point. For our 0.4-cm sample length, $L/b=0.2$. At $z_0=0$ (minimum waist in the center of the sample) the maximum number of ions excited increases only twofold for focusing tighter than $L/b\simeq 1$. Because the local electric field strength scales as b^{-2}, smaller values of b will only cause unwanted Stark mixing as well as surface and bulk damage with little increase in signal.

To measure the two-photon cross section, we use $z_0=0$ and Eq. (5) becomes

$$N=\frac{2T\rho\sigma P^2}{\lambda}\tan^{-1}\left[\frac{L}{b}\right] . \tag{6}$$

The peak voltage per laser pulse measured across the in-

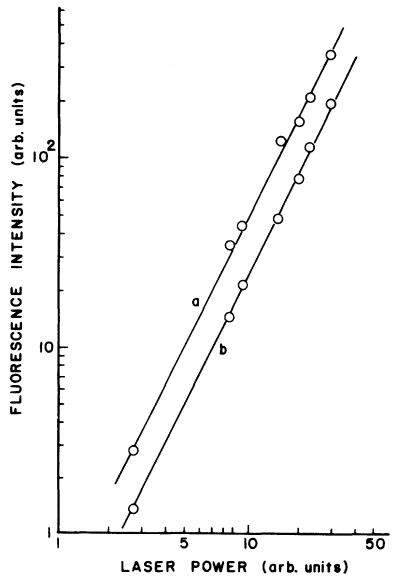

FIG. 4. Dye-laser power dependence of the Ce^{3+} emission. Each point represents the average of five measurements each of which has been averaged over 100 laser pulses. The straight lines have a slope of 2.0. The upper curve is for excitation of the no-phonon transition, the lower curve is for excitation at 615 nm into the phonon sideband.

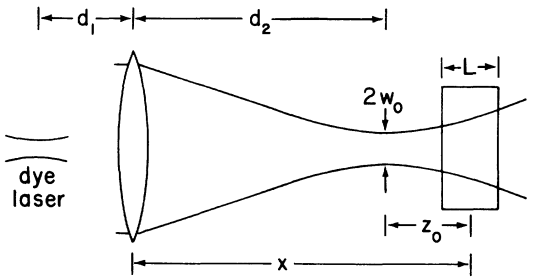

FIG. 5. Focusing geometry for the measurement of the effective waist w_0. The dye laser to lens separation d_1 is 320 cm.

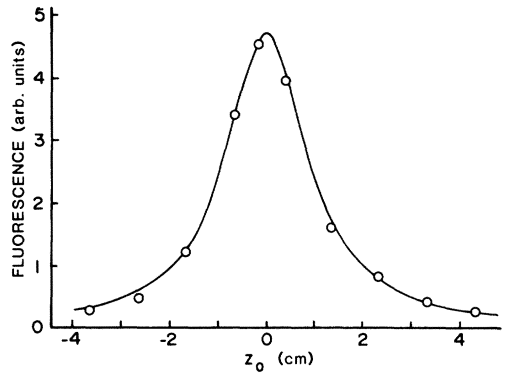

FIG. 6. Dependence of the fluorescence signal on the sample-to-waist separation z_0.

tegrating capacitor at the photomultiplier anode is

$$V = Q(\Delta\Omega/4\pi)\alpha q v N \ , \tag{7}$$

where the fluorescence quantum efficiency Q is taken to be unity,[22] the geometrical collection efficiency $\Delta\Omega/4\pi$ is 0.02, the quantum efficiency q of the photomultiplier cathode is 0.2, the voltage v per photoelectron from the photocathode is 25 mV, and α represents losses at air-glass interfaces and through the three uv transmitting filters and is of order 0.5. The dye-laser energy was maintained at about 0.2 mJ per 5-nsec pulse or 1.3×10^{23} photons/sec. This gives an intensity at the sample of 1.8 GW/cm^2. For a 0.003% sample the Ce^{3+} density is nominally 7.2×10^{16}/cm^3. At the no-phonon line in Fig. 3 the peak voltage across the integrating capacitor is 3.6 V. Combining these parameters with Eqs. (6) and (7), the peak cross section is approximately $\sigma = 2\times10^{-54}$ cm^{4}sec. We estimate a factor-of-5 uncertainty in the value of this number.

C. Polarization measurements

The polarization dependence of the two-photon absorption rate in solids has been treated theoretically by several authors.[23–25] The formalism developed has been applied to the case of impurity-ion–doped crystals.[2,3,9,11] The site symmetry of the impurity ion in the crystal determines the partial transition probabilities that are involved for a particular two-photon absorption.

For the Ce^{3+} ion in CaF_2 with site symmetry C_{4v}, the combinations contributing to the total transition probability are A_1, A_2, B_1, B_2, and E. Using the group-theoretical formalism from Bader and Gold,[24] we have calculated the dependence of the two-photon transition rate on the directions of the electric field vector $\hat{e}$ and the wave vector $\vec{k}$ of the incident laser beam. Since both the photons are derived from the same dye-laser field, their polarization and wave vectors are identical. The local tetragonal field around the Ce^{3+} ion is induced by an F^- charge compensator, which has an equal probability of going into an interstitial site along any of the [100], [010], or [001] directions of the host crystal. So the partial transition probabilities were calculated for all three possibilities and then averaged. The angle-dependent functions are linear combinations of these averaged partial transition probabilities and are presented in Table I. No attempts were made to assess the relative strengths of the different contributions.

In Fig. 7 we show the measured polarization dependence of the cross section at the no-phonon line along with the predictions from Table I. The Ce^{3+} concentrations in the [100], [110], and [111] oriented samples were 0.003%, 0.05%, and 0.1% respectively. The polarization measurement was repeated for a [100]-oriented sample with a 0.1% concentration. The polarization anisotropy at the no-phonon line was found to be completely independent of the Ce^{3+} concentration. However, the effect of concentration does become evident in the width of the no-phonon line. For the [100]-oriented samples, the FWHM of the no-phonon transition at 6 K increased from 0.64 cm^{-1} at 0.003% to 2.2 cm^{-1} at 0.1%. We attribute this change to the strain broadening introduced by the increased cerium and charge compensator density.

For the phonon sideband, the polarization dependence changes from that on the no-phonon line. In Fig. 8 we show the two-photon excitation spectrum taken under the same conditions as that in Fig. 3, except that the laser field is polarized at 45° to the CaF_2 [010] axis. To illustrate any anisotropy in the phonon sideband, we have subtracted the spectrum of Fig. 3 from this spectrum and the difference spectrum over the sideband is shown in the lower part of Fig. 8. At small frequency shifts from the position of the no-phonon line, the difference spectrum reveals that some of the structures in the sideband are highly anisotropic while others remained equal in strength. For large frequency shifts, the difference is seen to be uniformly zero suggesting that the cross section in this region is isotropic. To confirm this, we measured the polarization dependence in the far sideband for the [100]-oriented crystals as was done for the no-phonon transition. The cross section in this region was found to be isotropic for the 0.003% concentration crystal but the higher 0.1% sample showed a weak but distinct anisotropy which may be attributed to contributions from other Ce^{3+} centers.[15]

IV. DISCUSSION

For a two-photon electric dipole transition, the transition matrix element vanishes unless the final and initial states have the same parity. For pure $4f$ and $5d$ configurations of the Ce^{3+} ion, a two-photon process between them should be forbidden. Since the Ce^{3+} ion is in a site which lacks inversion symmetry, the static tetragonal

TABLE I. Calculated dependence for the absorption of two identical linearly polarized photons at a site of C_{4v} symmetry. The $\vec{k}$ vector has a fixed direction for a particular sample orientation as $\hat{e}$ is rotated through a variable angle θ measured from the indicated reference direction. The coefficients for the cross section are functions of the photon frequency and of the matrix elements between states participating in the transition.

$\vec{k}$	$\theta=0$	$\sigma(\theta)$
$\vec{k}\|\|[100]$	$\hat{e}\|\|[010]$	$a_1+b_1\sin^2 2\theta$
$\vec{k}\|\|[110]$	$\hat{e}\|\|[001]$	$a_2+b_2\sin^2 2\theta+c_2\sin^2\theta$
$\vec{k}\|\|[111]$	$\hat{e}\|\|[1\bar{1}0]$	a_3

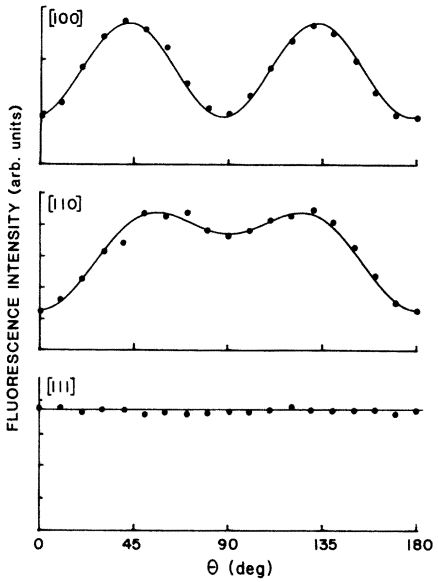

FIG. 7. Polarization dependence of the two-photon cross section for the no-phonon transition at a 6-K sample temperature. The solid circles represent the experimental measurements and the curves are fits to the data using the angular functions of Table I.

crystal potential will contain an odd component V_u. This odd crystal-field term will mix states of opposite parity and is responsible for the strength of the two-photon transition at the no-phonon line.[26] The initial and final states will then be mixtures of the $4f$ and $5d$ electronic orbitals possibly with components from the $6p$ and charge-transfer bands.[27,28] At the peak of the no-phonon line the cross section was measured to be approximately 5×10^{-54} cm^4 sec. Typical values for the cross section for an allowed two-photon transition[29] are of order $10^{-49}-10^{-51}$ cm^4 sec implying the only partially allowed nature of the two-photon transition for the Ce^{3+} ions. We have also integrated the measured two-photon cross section over the entire (313—295)-nm band. The value of this integrated cross section is of order 5×10^{-52} cm^4 sec cm^{-1} for energy units of cm^{-1}. We expect that $4f\rightarrow5d$ two-photon transitions in other lanthanide-doped systems will be of similar strength.

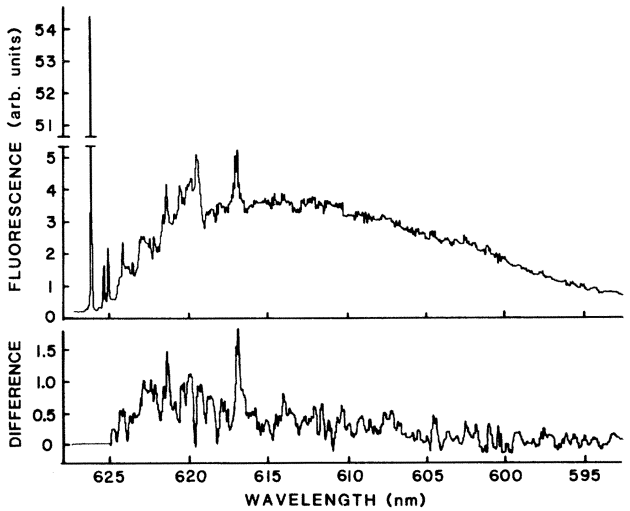

FIG. 8. Two-photon excitation spectrum where the laser is polarized at 45° to the [010] axis. The scale for the fluorescence intensity is the same as that in Fig. 3. The lower curve is the difference spectrum over the sideband and shows a wavelength-dependent polarization anisotropy.

Since the Ce^{3+} ion is at a noncentrosymmetric site, one expects that both even and odd vibrational modes will appear in the sideband for the two-photon transition. A comparison of the sidebands for the one-photon excitation and absorption spectra with the two-photon excitation spectra shows the one-to-one correspondence between the vibrational components. However, there are marked differences between the spectra in the relative sizes of the no-phonon line to the sideband as a whole, as well as in the relative strengths of the various sideband components.

The excellent agreement of the measured polarization dependence of the no-phonon cross section with the calculated angular functions confirms the C_{4v} symmetry of the Ce^{3+} site studied in this investigation. We also note that the averaging of the partial transition probabilities for the three possible orientations of the charge compensator is required to obtain the correct angular dependence. However, the situation in the sideband is more complex.

The regions in the sideband for the low-concentration samples where the polarization dependence was measured to be isotropic are at frequency shifts corresponding to multiphonon coupling to the Ce^{3+} ion. This isotropy can be understood by noting that the superimposed contributions from two or more vibrations with, in general, different symmetries average out the angular variations.

At smaller frequency shifts, closer to the no-phonon line, the difference spectrum in Fig. 8 reveals that the polarization anisotropy varies significantly with the phonon frequency. As is well known, both local modes of vibration involving the dopant ion and its close neighbors and the phonon modes of the host crystal which couple to the dopant ion may contribute to the phonon sideband. The polarization anisotropy at a particular phonon frequency in the sideband will thus depend on the symmetry of the phonon mode involved. A prominent feature in the one-photon excitation and absorption spectra is seen at a frequency shift of 490 cm^{-1} from the no-phonon line. This structure is also present in the 45° two-photon spectrum but is much weaker in the 0° scan and shows up as the dominant peak in the difference spectrum. Such a feature in the one-photon absorption spectrum of Ce^{3+}:CaF_2 has been identified[30,31] as a symmetric local mode of the fluorine ions surrounding the cerium site. The cross section for this mode above its background increases by about a factor of 3 in going from the 0° spectrum to the 45° spectrum. Since the no-phonon line increases by a factor of 2.7 between the same two polarizations, the cross section for this particular mode seems to scale with the cross section of the no-phonon transition as would be expected for a symmetric breathing mode.

V. CONCLUSIONS

The two-photon absorption from a $4f$ ground state to the lowest $5d$ state in Ce^{3+}:CaF_2 has been studied as a

function of laser wavelength, intensity, polarization, and focusing geometry. The two-photon nature of the process has been confirmed by measuring the dependence of the Ce^{3+} fluorescence strength on the dye-laser power. A sharp no-phonon line was observed when the dye-laser wavelength was exactly twice the wavelength for the one-photon resonance. The measured polarization dependence of the no-phonon line is consistent with a Ce^{3+} ion at a C_{4v} symmetry site. The two-photon cross section at the no-phonon line is of order 5×10^{-54} cm^4 sec, which indicates that the tetragonal crystal field is effective in mixing other parity states into the $4f$ and $5d$ configurations. The polarization dependence of the two-photon cross section in the sideband is a function of the symmetry of the participating phonons but is, in general, much more isotropic than that for the no-phonon transition.

ACKNOWLEDGMENTS

We wish to acknowledge the financial support of The University of Connecticut Research Foundation and The United States Department of Energy under Contract No. DE-AC02-82ER12012. We also thank Professor L. A. Kappers for the loan of pieces of equipment and Professor R. H. Bartram for several discussions.

[1]W. Kaiser and C. G. B. Garret, Phys. Rev. Lett. 7, 229 (1961).
[2]E. Bayer and G. Schaak, Phys. Status Solidi 41, 827 (1970).
[3]D. Frohlich, B. Staginnus, and S. Thurm, Phys. Status Solidi 40, 287 (1970).
[4]P. A. Apanasevich, R. I. Gintoft, V. S. Korolkov, A. G. Makhanek, and G. A. Skripko, Phys. Status Solidi B 58, 745 (1973).
[5]U. Fritzler, Z. Phys. B 27, 289 (1977).
[6]A. G. Makhanek and G. A. Skripko, Phys. Status Solidi A 53, 243 (1979).
[7]M. Dagenais, M. Downer, R. Neumann, and N. Bloembergen, Phys. Rev. Lett. 46, 561 (1981).
[8]M. A. Kramer and R. W. Boyd, Phys. Rev. B 23, 986 (1981).
[9]M. D. Downer, A. Bivas, and N. Bloembergen, Opt. Commun. 41, 335 (1982).
[10]W. M. Yen, C. G. Levy, S. Huang, and S. T. Lai, J. Lumin. 24/25, 659 (1982).
[11]S. A. Payne, A. B. Goldberg, and D. S. McClure, J. Chem. Phys. 78, 3688 (1983).
[12]E. Loh, Phys. Rev. 154, 270 (1967).
[13]W. J. Manthey, Phys. Rev. B 8, 4086 (1973); Ph.D. thesis, University of Chicago, 1972 (unpublished).
[14]T. Szczurek, G. F. W. Drake, and M. Schlesinger, Phys. Rev. B 8, 4910 (1973).
[15]K. W. Blazey and E. Loh, J. Phys. C 12, 3871 (1979).
[16]J. M. Baker, E. R. Davis, and J. P. Hurrel, Proc. R. Soc. London Ser. A 308, 403 (1968).
[17]M. J. Weber and R. W. Bierig, Phys. Rev. 134, A1492 (1964); M. J. Weber, R. W. Bierig, and S. I. Warsharo, *ibid.* 134, A1504 (1964).
[18]M. H. Crozier, Phys. Rev. 137, A1781 (1965).
[19]A. A. Kaplyanskii and V. N. Medvedev, Opt. Spectrosk. 23, 743 (1967) [Opt. Spectrosc. (USSR) 23, 404 (1967)].
[20]Since the sample radius is very large compared to the size of the laser beam we have let the upper limit on the radial integral go to infinity.
[21]E. H. A. Granneman and M. J. van der Weil, Rev. Sci. Instrum. 46, 332 (1975).
[22]M. J. Weber, Solid State Commun. 12, 741 (1973).
[23]M. Inoue and Y. Toyozawa, J. Phys. Soc. Jpn. 20, 363 (1965).
[24]T. R. Bader and A. Gold, Phys. Rev. 171, 997 (1968).
[25]M. M. Denisov and V. P. Makarov, J. Phys. C 5, 2651 (1972).
[26]The role played here by V_u is similar to that for the $4f \rightarrow 4f$ one-photon transitions in the rare earths.
[27]R. R. Jacobs, W. F. Krupke, and M. J. Weber, Appl. Phys. Lett. 33, 410 (1979).
[28]W. J. Miniscalco, J. M. Pellegrino, and W. M. Yen, J. Appl. Phys. 49, 6109 (1979).
[29]H. Mahr, in *Quantum Electronics, Vol. I: Nonlinear Optics,* edited by Herbert Rabin and C. L. Tang (Academic, New York, 1975), p. 287.
[30]W. Hayes, M. C. K. Wiltshire, W. J. Manthey, and D. S. McClure, J. Phys. C 6, L273 (1973).
[31]M. Schlesinger and G. W. F. Drake, Can. J. Phys. 54, 1699 (1976).